

Final Draft
of the original manuscript:

Okulov, I.V.; Okulov, A.V.; Soldatov, I.V.; Luthringer, B.; Willumeit-Roemer, R.; Wada, T.; Kato, H.; Weissmueller, J.; Markmann, J.:

Open porous dealloying-based biomaterials as a novel biomaterial platform

In: Materials Science and Engineering C 88 (2018) 95 - 103

First published online by Elsevier: March 15, 2018

DOI: 10.1016/j.msec.2018.03.008

<https://dx.doi.org/10.1016/j.msec.2018.03.008>

Open porous dealloying-based biomaterials as a novel biomaterial platform

I.V. Okulov^{a,b,*}, A.V. Okulov^a, I.V. Soldatov^{c,d}, B. Luthringer^e, R. Willumeit-Römer^e, T. Wada^b, H. Kato^b,
J. Weissmüller^{a,f}, and J. Markmann^{a,f}

^aHelmholtz-Zentrum Geesthacht, Institute of Materials Research, Division of Materials Mechanics, Geesthacht, Germany

^bInstitute for Materials Research, Tohoku University, Katahira 2-1-1, Sendai 980-8577, Japan

^cIFW Dresden, Helmholtzstraße 20, D-01069 Dresden, Germany

^dInstitute of Natural Sciences, Ural Federal University, 620000 Ekaterinburg, Russia

^eHelmholtz-Zentrum Geesthacht, Institute of Material Research, Division of Metallic Biomaterials, Geesthacht, Germany

^fHamburg University of Technology, Institute of Materials Physics and Technology, Hamburg, Germany

*Corresponding author; E-mail: ilya.okulov@hzg.de

Keywords: Dealloying; Porous material; Biomaterials design; Mechanical property; TiZr.

Abstract

The close match of stiffness between implant material and bone is critically important to avoid stress-shielding effect and ensure a fast healing of injured tissues. Here, we introduce liquid metal dealloying method for synthesis of robust open porous biomaterials possessing low Young's modulus. The remarkable advantage of the liquid metal dealloying method is a large flexibility in selecting chemical composition of a desired porous biomaterial together with unique tunable microstructure. To demonstrate the versatility of the method, a number of open porous $\text{Ti}_x\text{Zr}_{100-x}$ alloys with different chemical compositions and microstructural characteristics was developed by dealloying precursor $(\text{Ti}_x\text{Zr}_{100-x})_y\text{Cu}_{100-y}$ alloys in liquid magnesium. The effects of the processing conditions and the precursors' chemical composition on the microstructure of the porous $\text{Ti}_x\text{Zr}_{100-x}$ as well as their mechanical behavior were discussed in detail. In particular, the porous $\text{Ti}_x\text{Zr}_{100-x}$ distinguish themselves due to a low and tunable stiffness ranging from 3.2 to 15.1 GPa and a rather high strength reaching up to 480 MPa. This unique combination of mechanical properties of the new open porous $\text{Ti}_x\text{Zr}_{100-x}$ alloys becomes even more interesting in view of preliminary biological tests highlighting their excellent cytocompatibility. Overall, the liquid metal dealloying provides an opportunity for designing a new biomaterials platform with flexible tunable functionality.

Introduction

Commercially pure titanium and titanium alloys are widely used metallic materials for bone trauma healing, because of their good mechanical performance, excellent biocompatibility, and high corrosion resistance [1,2]. This, particularly, led to an increasing interest in the development of new titanium-based materials with improved performance over the past years [3–11]. Despite the success of existing commercial implant materials (including titanium alloys) in many cases, there is a risk of bone degeneration and implant loosening caused by the so-called “stress-shielding” effect [1,2]. The “stress-shielding” effect is associated with the disproportional load distribution between a bone and an adjacent implant due to their stiffness mismatch. The metallic implant materials are usually considerably stiffer as compared to bones. Eventually, the stiffness mismatch may lead to bone resorption and loosening or failure of the implant. There are several effective strategies to develop high-strength and low stiffness titanium alloys, for example, by designing multicomponent beta-titanium alloys [12–14], synthesis of complex microstructures [15–19] or introducing porosity into the material [20–22]. In this work, we followed the last strategy, namely, synthesis of porous titanium alloys by liquid metal dealloying.

Liquid metal dealloying method [23], invented in the group of Prof. H.Kato, is a metallurgical process for the synthesis of open porous materials by means of alloy corrosion in a liquid metal. The method employs diffusion of a liquid metal suited as a corrosive medium into a solid alloy accompanied by selective dissolution of one or more components of the alloy. The remaining part of the alloy is immiscible with the corrosive medium and rearranges into a continuous scaffold consisting of interconnected and dangling ligaments. The liquid metal dealloying method was used for fabrication of open porous materials such as Ti [22–24], Fe [25], Zr [22], Cr [25], Nb [26], TiNb [22], TiHf [27], C [28] as well as bicontinuous composites consisting of immiscible metals, namely, Ta-Cu [29] and Ti-Mg [23]. Synthesis of porous structures usually requires an additional fabrication step by which the corrosive medium itself is dissolved. For the bicontinuous composites, this step is simply omitted. The size of structural units of the liquid metal dealloying-based materials can be effectively tuned from nano- to micrometer range by control of the processing conditions [26,30,31]. Moreover, the liquid metal dealloying method can be employed to create nanoporous surface layers on the biomedical alloys to improve their biocompatibility. Thus, Fukuzumi and co-authors reported surface improvement of the widely applied in medicine Ti-6Al-4V alloy by selective removing of toxic aluminum (Al) using the liquid metal dealloying [32]. This is important since the implant surface influences bone metabolism and, therefore, osseointegration. Rougher surfaces stimulate differentiation, growth, and attachment of bone cells and increase mineralization leading to a better osseointegration [33]. Thus, the liquid metal dealloying method turns to be a powerful tool for creating complex metallic biomaterials with specific properties.

Here, we report design, synthesis and structure-property correlation of high-strength titanium-zirconium ($\text{Ti}_x\text{Zr}_{100-x}$) open porous scaffolds. The selection of $\text{Ti}_x\text{Zr}_{100-x}$ alloys for this study was governed by its excellent biocompatibility, good corrosion resistance, and superior strength compared to pure titanium [34]. Developed by dealloying in liquid magnesium, these new $\text{Ti}_x\text{Zr}_{100-x}$ scaffolds inherited a unique bicontinuous microstructure through manufacturing leading to outstanding mechanical behavior. Particularly, even at high solid fractions, Young’s modulus of these strong porous $\text{Ti}_x\text{Zr}_{100-x}$ scaffolds remains in a range of that of cortical bone providing the opportunity of precise stiffness adjustment between implant and bone. Both microstructural and mechanical characterizations together with preliminary cytotoxicity analysis of these porous $\text{Ti}_x\text{Zr}_{100-x}$ solids are discussed in details.

Materials and methods

Alloys design

Precursor alloys for the liquid metal dealloying were designed based on the enthalpy of mixture values between Mg and the considered alloy element ($\Delta H_{(Mg-element)}^{mix}$) [35] as well as on biocompatibility of the alloying elements [2,36–40]. Elements exhibiting a negative value of $\Delta H_{(Mg-element)}^{mix}$ like Al, Si, Cu or Ni are miscible and will be dissolved in Mg upon the dealloying process while those possessing a positive $\Delta H_{(Mg-element)}^{mix}$ like Ti, Zr, V or Fe are immiscible in Mg. According to Fig. 1, the choice of elements, which are both biocompatible and immiscible in Mg, includes Ti, Zr, Nb, Mo, Hf, and Ta. We have selected Ti and Zr as immiscible and Cu as miscible elements for our alloy design. The first set of designed alloys, namely, $Ti_{15}Zr_{15}Cu_{70}$, $Ti_{20}Zr_{20}Cu_{60}$, $Ti_{25}Zr_{25}Cu_{50}$ and $Ti_{30}Zr_{30}Cu_{40}$ (at.%) was chosen in order to identify the parting limit (the lowest concentration of Cu at which dealloying is still progressing) as well as to study the effect of the Ti_xZr_{100-x} solid fraction on the mechanical response. The second set of samples, namely $Ti_{20}Zr_{20}Cu_{60}$, $Ti_{10}Zr_{30}Cu_{60}$, $Ti_{30}Zr_{10}Cu_{60}$ (at.%), was chosen to study the effect of solid solution strengthening in the porous Ti_xZr_{100-x} samples.

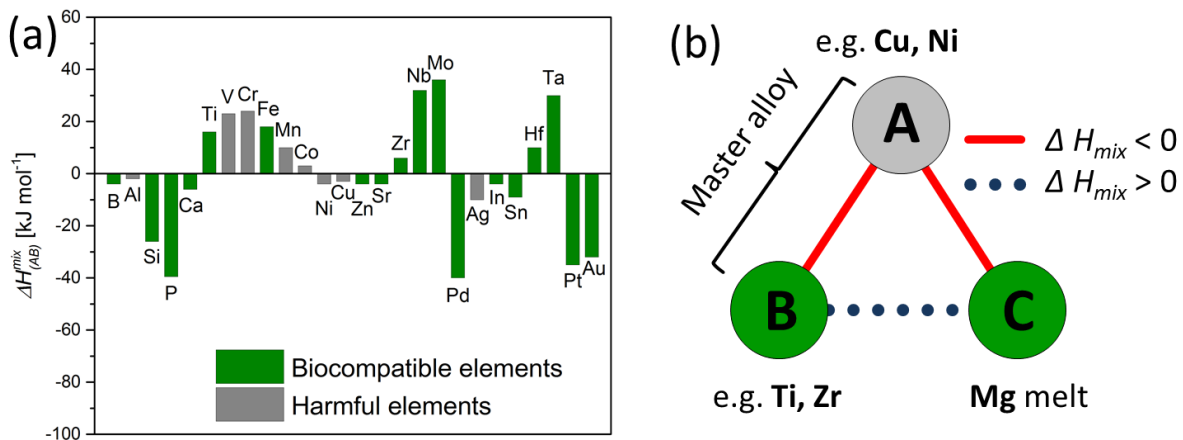


Figure 1 Selection of elements for dealloying in a liquid metal. (a) The values of $\Delta H_{(AB)}^{mix}$ (kJ/mol) calculated by Miedema's model for atomic pairs between Mg and elements indicated in the plot [35]; (b) Required relationship of the values of enthalpy of mixing between elements for the liquid metal dealloying of a master alloy AB in a liquid metal C.

Fabrication method

Rods 1 mm in diameter were prepared from pure metals (99.99 %) by an arc melting device coupled with a suction casting set-up under argon (Ar) atmosphere (Mini Arc Melter MAM-1, Edmund Bühler, Germany). The as-cast rods were cut to 1.7 mm length by a horizontal diamond wire saw (Model 3032, Well Diamantssägen, Germany). These 1.7 mm long rods were then systematically heated for various times and temperatures together with ~ 130 mg magnesium (Mg) (-12+50 mesh) in a glassy carbon crucible under Ar flow using an infrared furnace (IRF 10, Behr, Switzerland). The infrared furnace was chosen due to high heating and cooling rates of about $\sim 40 \text{ K s}^{-1}$. The schematic illustration of the dealloying set-up is shown in Fig. 2 a. All mechanically tested samples had the same process parameters, i.e. dealloying at 1023 K for 10 min. For investigation of the synthesis procedure itself, also different times and temperatures were chosen. Upon dealloying, molten Mg selectively dissolves Cu out of the parent $(\text{Ti}_x\text{Zr}_{100-x})_y\text{Cu}_{100-y}$ alloys, while Ti and Zr diffuse along the metal/liquid interface [23,41]. After dealloying, the samples consist of hexagonal close-packed (hcp) Ti or hcp $\text{Ti}_x\text{Zr}_{100-x}$, and Mg-rich phases, which depend on the used precursor alloy. In order to obtain the porous samples, the Mg phase(s) were removed by etching in 3 M HNO_3 for 5h as shown in Fig. 2 b.

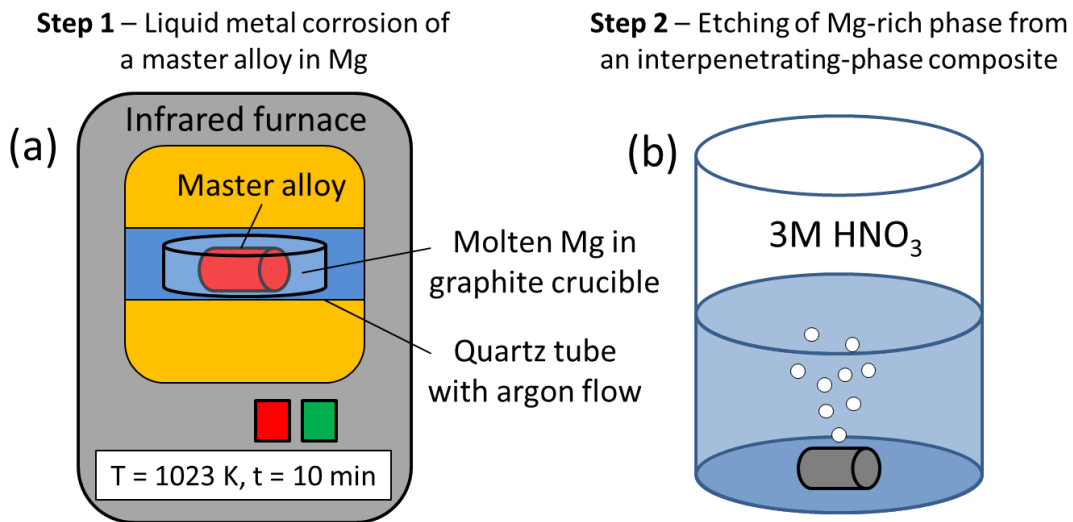


Figure 2 Schematic illustration of fabrication of porous metals by liquid metal dealloying

Characterization methods

Structural investigation of the precursor alloys and porous samples was performed by X-ray diffraction in Bragg-Brentano geometry (D8 Advance, Bruker, Germany) with Cu-K α radiation. The device was equipped with position sensitive detector (LynxEye, Bruker, Germany) enabling us to achieve acceptable signal-to-noise ratios within a few hours measuring time despite the smallness of the samples. Scanning electron microscopy (SEM, Nova Nanolab 200, FEI, USA, and Tescan Vega3 SB, Czech Republic) coupled with energy-dispersive X-ray analysis explored microstructure and composition. The samples' volume before and after dealloying was measured by a micrometer screw gauge and SEM. The further structural parameters such as volume fraction, ϕ , and density, ρ , of the porous alloys were calculated based on the measured values of samples' volume and weight. The porous samples were tested in compression at room temperature with an applied (engineering) strain rate of 10^{-4} s^{-1} using a universal testing device (Z010 TN, Zwick-Roell, Germany). The shape of tested porous samples was cylindrical with 1 mm in diameter and 1.7 mm in length. The strain was computed from the relative displacement of the load surfaces, as measured by a laser extensometer (LaserXtens, Zwick). The yield strength of the porous metals and composites was determined as the stress at 0.002 offset strain.

Cytocompatibility test

Human umbilical cord perivascular cells (HUCPV) were isolated with the approval from the local ethical committee Ethik-Kommission der Ärztekammer Hamburg (Hamburg, Germany), following the protocols from Sarugaser *et al.* [42]. HUCPV were obtained from umbilical cord samples. Written informed consent from the donor was obtained for the use of these samples in research. The cord was cut into pieces of about 5 cm. The vessels were then isolated and tied together at the ends, leading to a vessel loop. Afterward, they were placed in T-175 cell culture flask and cultured for 10 days in α -minimum essential medium (α -MEM; Fisher Scientific GmbH, Schwerte, Germany) and 15% fetal bovine serum (FBS; Biological industries - NeoFroxx, Einhausen, Germany) and 1% antibiotics. After outgrowth of cells from the tissues, the medium was changed every 2–3 days.

For each assay, samples (beforehand cleaned and sterilized in 70% ethanol for 20 min in an ultrasonic bath) were placed into an agarose pre-coated 12-well plate. Mirror-polished nonporous Ti6Al4V disc-shaped samples with a diameter of 10 mm were employed as reference specimen (cut from a round bar (F. W. Hempel Legierungsmetall GmbH & Co.KG, Oberhausen, Germany)), polished by conventional procedures followed by final manual polishing with a Struers oxide polish suspension (OPS) compound (Struers GmbH, Hannover-Garbsen, Germany). The porous Ti $_x$ Zr $_{100-x}$ flat samples were fabricated by the dealloying method described above in the section "Fabrication method". The dealloying parameters were 1000 K and 10 min. The size of the Ti $_x$ Zr $_{100-x}$ samples was 1 mm X 5 mm x 5 mm. Afterward 5000 cells in 6 μL were added to each sample and incubated for 30 min to allow early cell adhesion. Then 3 mL of fresh medium was added to each well. Cells were further cultured for 5 days with a medium change in between.

In vitro qualitative analysis of material cytotoxicity was performed by using a LIVE/DEAD (Life technologies, Darmstadt, Germany) assay. After 5 days culture, the staining solution was prepared by adding 4 μL Calcein AM (LIVE - green), and 10 μL Ethidium homodimer-1 (DEAD - red) to 10 mL of phosphate-buffered saline (PBS). The samples were first washed with PBS to eliminate non-adherent cells, followed by immersion of each sample in 1.5 mL of staining solution, and incubating them under cell

culture conditions. The staining solution was then replaced by fresh α -MEM and samples were visualized by the fluorescent microscope (Nikon GmbH, Düsseldorf, Germany).

Results

The dealloying of the designed $(\text{Ti}_x\text{Zr}_{100-x})_y\text{Cu}_{100-y}$ precursor alloys in liquid Mg with following etching resulted in the formation of porous-structured samples. Hereafter, these porous samples fabricated from the $(\text{TiZr})_{30}\text{Cu}_{70}$, $(\text{TiZr})_{40}\text{Cu}_{60}$, $(\text{TiZr})_{50}\text{Cu}_{50}$, and $(\text{TiZr})_{60}\text{Cu}_{40}$ precursors are referred as TiZr@49vol%, TiZr@63vol%, TiZr@68vol%, and TiZr@79vol%, respectively. The porous samples fabricated from the $\text{Ti}_{30}\text{Zr}_{10}\text{Cu}_{60}$ and $\text{Ti}_{10}\text{Zr}_{30}\text{Cu}_{60}$ are referred as $\text{Ti}_{75}\text{Zr}_{25}$ @70vol% and $\text{Ti}_{25}\text{Zr}_{75}$ @58vol%, respectively. The number indicates the metal volume fraction, φ , and for convenience this is reflected in [Table 1](#). The volume fraction values were calculated based on measured values of volume and weight. The dealloyed samples inherit the cylindrical shape of their precursors' alloys.

Microstructure of the open porous $\text{Ti}_x\text{Zr}_{100-x}$ alloys

After dealloying of the $(\text{Ti}_x\text{Zr}_{100-x})_y\text{Cu}_{100-y}$ precursors with following etching the final $\text{Ti}_x\text{Zr}_{100-x}$ -based porous samples mainly consist of Ti and Zr which are homogeneously distributed ([Fig. 3 a](#)). Additionally, there are traces of remaining Cu that is below 1 at. % as identified by EDX analysis. The X-ray diffraction analysis of the porous $\text{Ti}_x\text{Zr}_{100-x}$ samples indicates that these are single phase alloys consisting of the hcp (hexagonal close-packed) α -TiZr phase as exemplified for the porous $\text{Ti}_{50}\text{Zr}_{50}$ in [Fig. 3 b](#).

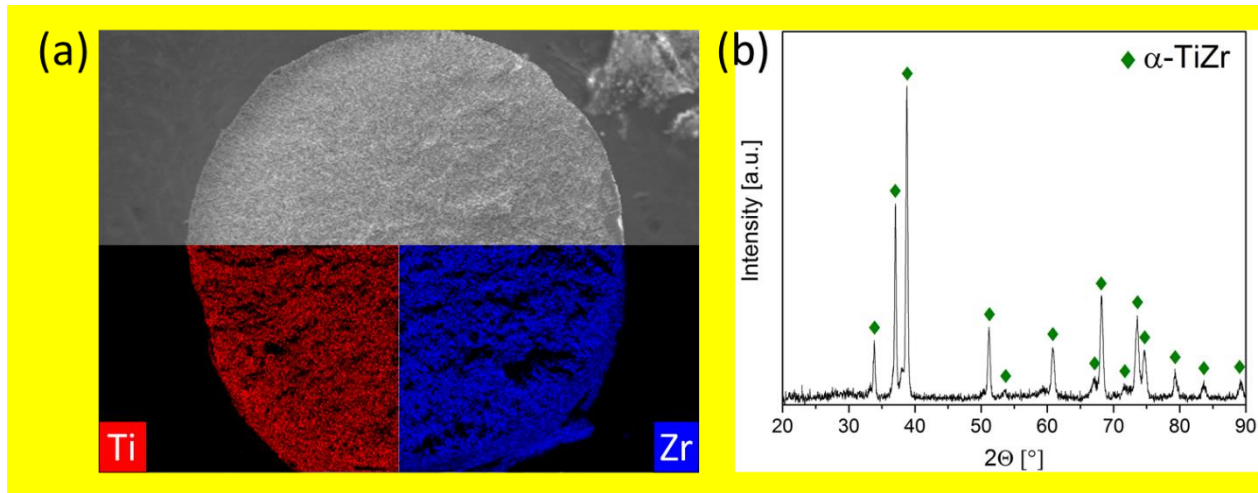


Figure 3 (a) Elemental mapping and (b) X-ray diffractogram of the porous $\text{Ti}_{50}\text{Zr}_{50}$. The diffractogram and elemental mapping are representative for the porous $\text{Ti}_x\text{Zr}_{100-x}$ synthesized in this study.

The SEM analysis reveals the porous structure of the developed $\text{Ti}_x\text{Zr}_{100-x}$ alloys. The corresponding SEM micrographs are shown in [Figs. 4-6](#). The set of SEM micrographs in [Fig. 4](#) summarizes the effect of processing parameters, namely, time and temperature, on the ligament size of the porous TiZr samples fabricated from the $(\text{TiZr})_{30}\text{Cu}_{70}$ precursor. The smallest ligament size of about $1.34 \pm 0.27 \mu\text{m}$ corresponds to a dealloying treatment at 1073 K for 5 min ([Fig. 4 a](#)). Increasing processing time while keeping the temperature constant (1073 K) leads to higher ligament size ([Figs. 4 b and c](#)), e.g. $1.94 \pm 0.34 \mu\text{m}$ and

$2.43 \pm 0.34 \mu\text{m}$ for 10 min and 20 min, respectively. The same trend is observed at increasing temperature but constant time. In particular, the ligament size of porous TiZr after 5 min of dealloying is $1.50 \pm 0.28 \mu\text{m}$ and $1.85 \pm 0.38 \mu\text{m}$ when the processing temperature is 1123 K and 1173 K, respectively. Thus, this set of micrographs is a clear evidence of microstructural design possibilities of the dealloying process of a single precursor alloy. A second example of microstructural design possibilities is the effect of initial composition, namely the Cu content in the master $(\text{TiZr})_x\text{Cu}_{100-x}$ alloys.

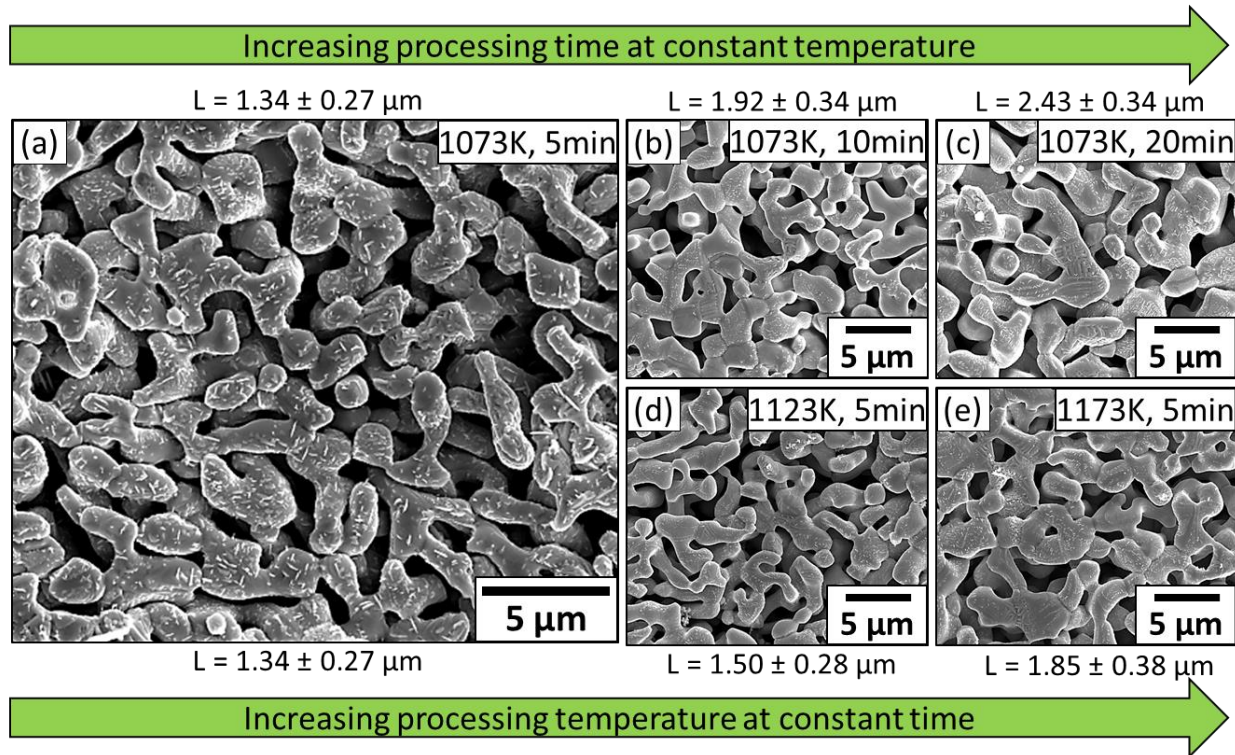


Figure 4 SEM micrographs of porous TiZr alloys fabricated from the $(\text{TiZr})_{30}\text{Cu}_{70}$ precursor by liquid metal dealloying at different processing parameters. (a) $T = 1073 \text{ K}$ and $t = 5 \text{ min}$; (b) $T = 1073 \text{ K}$ and $t = 10 \text{ min}$; (c) $T = 1073 \text{ K}$ and $t = 20 \text{ min}$; (d) $T = 1123 \text{ K}$ and $t = 5 \text{ min}$; (e) $T = 1173 \text{ K}$ and $t = 10 \text{ min}$. Note: L indicates the size of ligaments.

The set of SEM micrographs in Fig. 5 summarizes the effect of the precursor composition on the microstructure of the porous TiZr samples. The samples are fabricated from different precursors but processed under the same conditions, namely, at 1023 K for 10 min. So, the ligament size difference from sample to the sample is not pronounced. The density estimations reveal that the significant difference of the fraction of solid phase between the samples (Table 1). A higher concentration of Cu in the precursors leads to a lower solid fraction in the porous samples. This can be explained by the fact that the dealloying process involves the selective dissolution of Cu into liquid Mg. The higher the Cu content is the higher the resulting porosity volume fraction. Another factor influencing the volume fraction of the solid phase in the porous TiZr is the shrinkage of samples upon dealloying. The shrinkage values vary from 7 to 17 vol% depending on the precursor's alloy composition. A higher concentration of Cu in the $(\text{TiZr})_x\text{Cu}_{100-x}$ precursors also leads to a larger shrinkage during dealloying (Table 1). For example, dealloying of

(TiZr)₃₀Cu₇₀ and (TiZr)₅₀Cu₅₀ leads to 15 vol% and 8 vol% shrinkage, respectively. But the resulting density of samples with higher initial Cu content is still lower despite the observed increase in densification. Thus, the control of initial Cu concentration in the (TiZr)_xCu_{100-x} precursors is an effective tool to design the porous TiZr scaffold with desired porosity volume fraction.

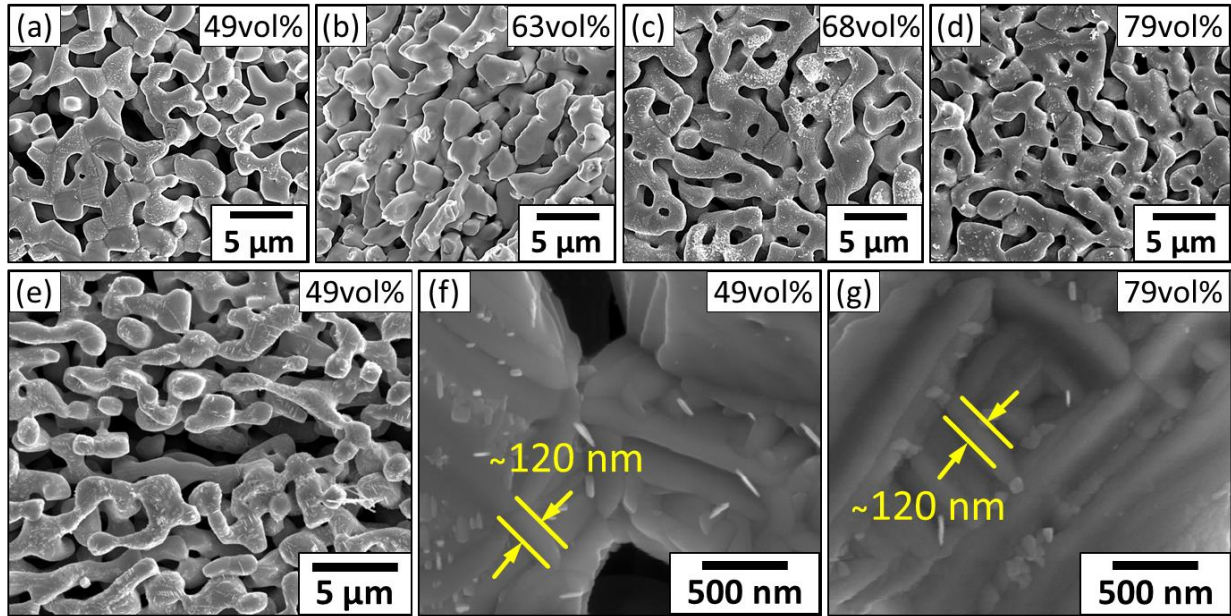


Figure 5 SEM micrographs of porous TiZr alloys fabricated from (TiZr)_xCu_{100-x} by liquid metal dealloying.

(a) TiZr@49vol% sample fabricated from (TiZr)₃₀Cu₇₀ at 1023 K for 10 min; (b) TiZr@63vol% sample fabricated from (TiZr)₄₀Cu₆₀ at 1023 K for 10 min; (c) TiZr@68vol% sample fabricated from (TiZr)₅₀Cu₅₀ at 1073 K for 10 min; (d) TiZr@79vol% sample fabricated from (TiZr)₆₀Cu₄₀ at 1023 K for 10 min; (e) Crack-like defect in the TiZr@49vol% sample; (f) and (g) Detailed microstructure of individual ligaments of the TiZr@49vol% and TiZr@79vol% samples, respectively, indicating ultrafine lamellae structure.

Table 1 Structural parameters of the porous TiZr. ϕ – volume fraction of the TiZr phase, ϕ_{porosity} – volume fraction of porosity, $\Delta V/V$ – relative volume shrinkage during dealloying, ρ - mass density.

Precursor alloy (at%)	Sample name	ϕ [no units]	ϕ_{porosity} [no units]	$\Delta V/V$ [vol%]	ρ [g cm ⁻³]
(TiZr) ₃₀ Cu ₇₀	TiZr@49vol%	0.49±0.05	0.51±0.05	15±3	2.8±0.1
(TiZr) ₄₀ Cu ₆₀	TiZr@63vol%	0.63±0.05	0.37±0.05	16±3	3.6±0.1
(TiZr) ₅₀ Cu ₅₀	TiZr@68vol%	0.68±0.05	0.32±0.05	8±3	3.8±0.1
(TiZr) ₆₀ Cu ₄₀	TiZr@79vol%	0.79±0.05	0.21±0.05	10±2	4.5±0.2
Ti ₁₀ Zr ₃₀ Cu ₆₀	Ti ₂₅ Zr ₇₅ @58vol%	0.58±0.05	0.42±0.05	17±3	4.1±0.2
Ti ₃₀ Zr ₁₀ Cu ₆₀	Ti ₇₅ Zr ₂₅ @70vol%	0.70±0.05	0.30±0.05	7±3	3.1±0.1

Before addressing the third example of the microstructural design of porous TiZr alloys, some interesting microstructural features exemplified in Fig. 5 has to be emphasized. Firstly, the detailed observation of

the sample's surface indicates the presence of large pores with elongated shape (Fig. 5 e) similar to crack-like defects in nanoporous gold [43]. The second and most distinguished microstructural feature of the porous TiZr alloys is the ultrafine lamellae microstructure of the individual ligaments. The lamellae or basket-weave microstructure is typical for titanium alloys [44,45]. Usually, such fine lamellae precipitate upon very fast cooling from the β phase field of titanium alloys. The body-centered cubic structure of the β phase leads to 12 variants of the orientation of these lamellae, but not all 12 possible variants are nucleated statistically. Instead, in order to minimize the overall elastic strains only two or three variants being nearly perpendicular to each other dominate in a given volume of a β phase [46]. In the current case, the lamellae thickness is in an ultrafine-scale regime of about 120 nm as can be seen in the SEM micrographs in Figs. 5 f-g. Based on this evidence, one can consider a control of the lamellae thickness by optimizing the cooling rate after dealloying or subjecting the porous scaffolds to post-dealloying heat-treatments.

Figs. 5 b and 6 presents the microstructure of several porous Ti_xZr_{100-x} alloys fabricated from precursor alloys with the same Cu concentration (60 at.%) and the same dealloying parameters (1023 K and 10 min). The increasing of the Zr content in this set of samples leads to a higher shrinkage of samples during dealloying and higher fraction of porosity in final porous samples (Table 1). SEM analysis indicates that the $Ti_{25}Zr_{75}$ and $Ti_{75}Zr_{25}$ samples consist of lamellar structures what was also observed for the $Ti_{50}Zr_{50}$ sample. However, the lamellae of the non-equilibrium compositions are coarser as compared to the case of the equilibrium one. Thus, tuning of the chemical composition of the precursor alloys, namely, ratio between Ti and Zr, enables manipulation of the Ti_xZr_{100-x} microstructure. In its turn, microstructure and chemical composition of the current porous Ti_xZr_{100-x} scaffolds significantly affect their stress-strain behavior reported below.

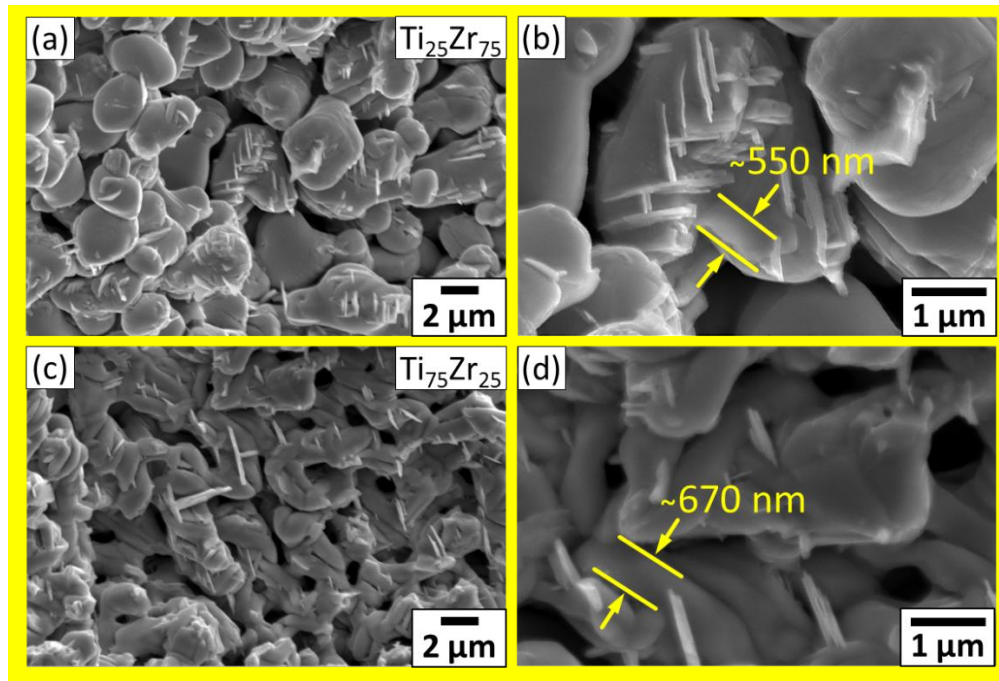


Figure 6 SEM micrographs of porous Ti_xZr_{100-x} alloys fabricated from $(Ti_xZr_{100-x})_yCu_{100-y}$ precursors by liquid metal dealloying at 1023 K for 10 min. (a and b) $Ti_{25}Zr_{75}$ sample fabricated from $Ti_{10}Zr_{30}Cu_{60}$; and (c and d) $Ti_{75}Zr_{25}$ sample fabricated from $Ti_{30}Zr_{10}Cu_{60}$. Note: compositions are given in at.%.

Mechanical properties of the microporous Ti_xZr_{100-x} alloys

An indubitable advantage of the dealloying-based porous Ti_xZr_{100-x} over their bulk counterparts in a view of implant application is that the current porous Ti_xZr_{100-x} alloys possess very low Young's modulus, Y . The Y value can be adjusted between 3.2 GPa to 15.1 GPa through control of solid fraction, ϕ (Fig. 7, Table 2). A higher Y value corresponds to a higher ϕ value. The remarkable result is that the low Y values go along with high yield strength, σ_y , values. The σ_y values of the current TiZr samples are in a range from 110 to 480 MPa (Table 1, Fig. 7 a), distinguishing these materials from other dealloying-based porous metals and alloys. In the same way as Y , the $\sigma_{0.2}$ of porous TiZr can be tuned by controlling ϕ as it is strongly dependent on the solid fraction (Fig. 7 a). In particular, the σ_y values of the dealloying-based porous Ti_xZr_{100-x} materials with ϕ values equal to 68 vol.% and 79 vol.% are about 321 MPa and 480 MPa, respectively.

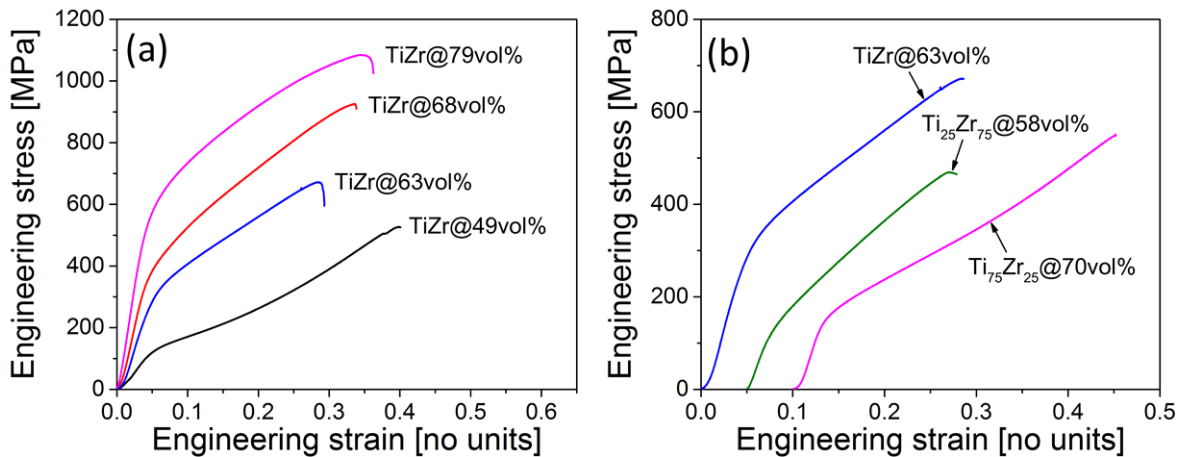


Figure 7 Mechanical properties of the porous TiZr samples under compressive loading. (a) Effect of solid fraction on mechanical properties for the porous TiZr alloy; (b) Effect of composition on mechanical properties for the TiZr, $Ti_{25}Zr_{75}$, and $Ti_{75}Zr_{25}$ (at%) alloys fabricated from the TiZrCu master alloys containing 60 at% of Cu. Note: the part of samples name before „@“ indicates alloy composition in at%, the part after „@“ indicates solid fraction of the sample“.

Table 2 Mechanical properties of the porous TiZr. Y – Young's modulus, $\sigma_{0.2}$ – yield strength.

Precursor alloy (at%)	Sample name	Y [GPa]	$\sigma_{0.2}$ [MPa]
$(TiZr)_{30}Cu_{70}$	TiZr@49vol%	3.2 ± 0.2	110 ± 10
$(TiZr)_{40}Cu_{60}$	TiZr@63vol%	7.3 ± 0.4	259 ± 25
$(TiZr)_{50}Cu_{50}$	TiZr@68vol%	10.4 ± 2	321 ± 35
$(TiZr)_{60}Cu_{40}$	TiZr@79vol%	15.1 ± 3	480 ± 35
$Ti_{10}Zr_{30}Cu_{60}$	$Ti_{25}Zr_{75}$ @58vol%	5.5 ± 0.5	117 ± 10
$Ti_{30}Zr_{10}Cu_{60}$	$Ti_{75}Zr_{25}$ @70vol%	6.2 ± 0.7	136 ± 10

Apart from appropriate strength and stiffness parameters, the load-bearing implant materials should possess reasonable deformability. The compression tests show that the current porous TiZr materials are, indeed, plastically deformable with strain values ranging from 0.2 to 0.4 (Fig. 7). This plastic deformation of the porous Ti_xZr_{100-x} samples is accompanied by a pronounced strain-hardening behavior what is partially due to a densification of the porous scaffold. The process of densification includes decreasing of interligament space and arrangement of ligaments perpendicular to the loading direction as demonstrated in Fig. 8 a. The SEM analysis of deformed samples also reveals the presence of local plastic deformation (Fig. 8 b) in form of numerous slip bands on the surface of the ligaments. These slip bands obviously are a result of dislocation motion due to plastic deformation. However, the most interesting finding was disclosed during fracture surface analysis. It seems that during plastic deformation under compressive loading, some ligaments were subjected to tensile loading. Regions of the fracture surface covered by dimples with a size less than 100 nm as can be seen in Fig. 8 c prove that some individual ligaments were ruptured apart in a purely ductile nature.

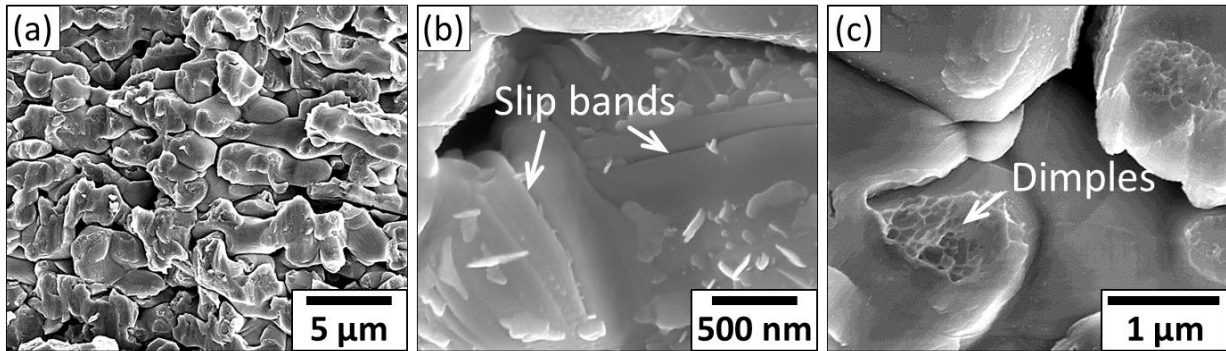


Figure 8 SEM micrographs of the deformed to fracture porous TiZr samples. (a) Compaction and alignment of ligaments perpendicular to the loading direction in TiZr@68vol% (loading direction is vertical); (b) Slip bands on the surface of individual ligaments in TiZr@49vol%; (c) Dimples on the fracture surface of the individual ligaments in TiZr@68vol%.

Cytocompatibility test

To ensure the initial cytocompatibility of the porous metals fabricated by the liquid metal dealloying, a LIVE/DEAD staining was performed after 5 days HUCPV culture. As Ti-6Al-4V is widely applied in biomedical application, it was selected as a comparison in order to be able to interpret the results. **Fig. 9** presents staining micrographs of a porous TiZr sample and of the Ti-6Al-4V alloy. Only a few red cells were detected on each sample (maybe less on the porous TiZr). However, compared to the polished surface of the Ti-6Al-4V (control) material, more viable (and spread) cells could be found on the rough surfaces of the porous TiZr material. The different cell response may be due to the different surface roughness and to the various chemical compositions of the studied materials. The rough surface of the porous materials is more favorable for cells adhesion compared to the polished one. This might even stimulate a better osseointegration behavior of the developed porous materials what is quite advantageous in view of the possible application as an implant material.

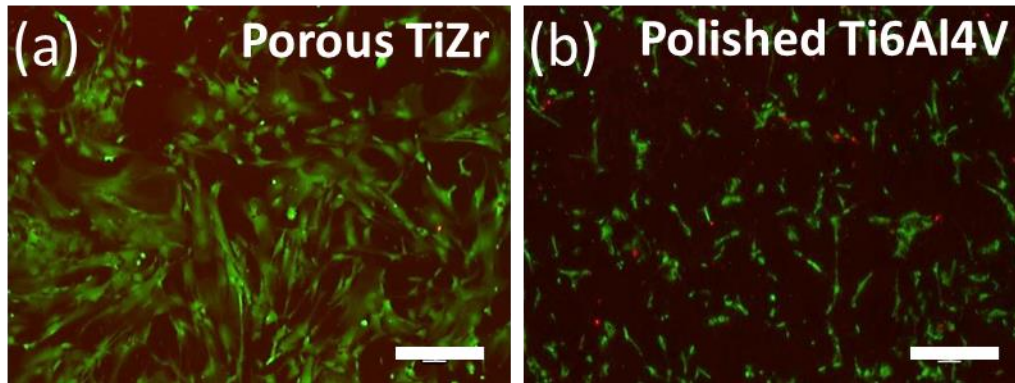


Figure 9 Fluorescence images of HUCPV cells cultured on porous TiZr (a) of the current study and Ti6Al4V alloy (b; control). Fluorescence LIVE (green)/DEAD (red) staining was performed after 5 days of cell culture. Scale bar 400 μm .

Discussion

Microstructure

The porous $\text{Ti}_x\text{Zr}_{100-x}$ alloys were successfully synthesized from the $(\text{Ti}_x\text{Zr}_{100-x})_y\text{Cu}_{100-y}$ precursor alloys with an atomic concentration of Cu varying from 40 to 70 at.%. Similar to the electrochemical dealloying, there is a critical alloy composition (referred also as parting limit) required for full dealloying in the liquid metal dealloying [30]. This characteristic is important for practical reasons as a lower Cu concentration in $(\text{Ti}_x\text{Zr}_{100-x})_y\text{Cu}_{100-y}$ leads to a higher solid fraction in the porous $\text{Ti}_x\text{Zr}_{100-x}$ alloys. The porous $\text{Ti}_x\text{Zr}_{100-x}$ alloys with higher solid fraction exhibit superior strength characteristics. In the current study, we did not study the parting limit in detail. However, dealloying of a precursor with the critical composition, namely the $\text{Ti}_{30}\text{Zr}_{70}\text{Cu}_{40}$ precursor, was limited to 1223 K. At higher temperatures, dealloying was not completed. We correlate these observations with a competing coarsening process of ligaments fusing together at higher dealloying temperatures and, therefore, blocking paths for Mg to diffuse into the precursor alloy. The similar parting limit – about 40 at.% – was reported by McCue et al. for rather different dealloying system, namely TiTa dealloyed in Cu [30]. The authors emphasized the extremely low parting limit in the case of the liquid metal dealloying compared to electrochemical dealloying. Our observations support this conclusion. However, we believe that further systematic investigations of different dealloying systems are required to support this statement.

To control the resulting ligament size of the dealloyed-based porous metals is essential for their structural as well as functional properties. For example, decreasing of ligament size of electrochemically fabricated nanoporous metals, usually noble ones such as nanoporous gold (NPG), leads to significantly higher strength[47]. Here, several bulk porous $\text{Ti}_x\text{Zr}_{100-x}$ commercial alloys were synthesized to demonstrate capabilities of the liquid dealloying method in tuning of ligament size. As it was shown, the ligament size of the current $\text{Ti}_x\text{Zr}_{100-x}$ alloys can be tuned from about one to several micrometers by varying processing parameters such as time and temperature as well as chemical composition of precursor alloys. Since the liquid metal dealloying is a diffusion-mediated process, there is a trade-of between sample thickness and final ligament size as demonstrated in [24,26]. High processing temperatures lead to significant ligament coarsening. On the other hand, reducing processing temperature results in an increase of processing time. Interestingly, the ligament size is depended on the precursor alloy composition like in the case of the $(\text{Ti}_x\text{Zr}_{100-x})_y\text{Cu}_{100-y}$ alloys with different Ti to Zr ratio. Comparison of the as-dealloyed microstructure of the $(\text{TiZr})_{30}\text{Cu}_{70}$ alloy with the previously reported $\text{Ti}_{30}\text{Cu}_{70}$ one [22] also supports this statement. This suggests additional opportunities for the ligament size control by optimization of the chemical composition of the precursor alloy.

In terms of mechanical performance, ligament size, solid fraction, and chemical composition significantly influence the strength and stiffness of porous materials. We now turn to discuss the mechanical properties of the current porous alloys with relation to their microstructure.

Mechanical behavior

The reported liquid metal dealloying-based porous alloys exhibit insufficient strength characteristics for orthopedic implant applications. For example, the maximum reached σ_y value for the porous Ti is about 72 MPa [22]. The required σ_y should be several times higher than the ultimate stress of cortical bone which is in the range between 50 and 150 MPa [48] in order to avoid damage of implant or/and bone during the healing process. The governing reason for the development of the porous Ti_xZr_{100-x} alloys was the improvement of strength performance of the dealloying-based porous alloys for biomedical applications. In this study, we investigated two approaches for optimization of mechanical properties, namely the tuning the solid fraction as well as the chemical composition.

The effect of the solid fraction on the mechanical behavior of the dealloying-based materials was reported for porous Ti in our previous investigation [22]. The same trend, namely the higher solid fraction leads to higher strength as well as stiffness, is observed for the current porous TiZr samples. Generally, the stiffness of dealloyed metals depends on the interconnectivity of ligaments network [49,50]. In its turn, the latter depends on the precursor alloy composition [30] and increases as this approaches the parting limit. Based on this statement, the increasing stiffness accompanied by increasing solid fraction (Fig. 7 a) is probably due to increasing interconnectivity of ligaments. However, the overall stiffness values of the porous TiZr reaching about 15 GPa are surprisingly low and are in the range of that for cortical bone. The low stiffness of the dealloying-based porous metals is due to the unique microstructure inherited from processing [22]. It can be readily concluded from the finding that the sintered porous metals exhibit higher stiffness values compared to the dealloying-based ones at the same porosity [10,51].

The interconnectivity of ligaments is also likely to affect the strength of the current porous TiZr alloys. However, the most exciting finding is a significant improvement of strength characteristics of the porous TiZr compared with the porous Ti from the previous studies [22,31]. Comparing σ_y values of TiZr@63vol% (259 MPa) with the porous Ti (72 MPa) [22] exhibiting similar φ values indicates more than three-fold strength improvement. The main reason for this improvement is the solid solution strengthening effect. The equiatomic TiZr alloy is known to be about 2.5 times stronger than pure Ti [34,44]. However, in accordance with the Hall-Petch relationship, the coarser ligament size of TiZr@63vol% as compared to the porous Ti should lead to somewhat lower strength improvement. We believe that a second significant strengthening mechanism of TiZr@63vol% lies in the ultrafine-grained microstructure of individual ligaments as exemplified in Figs. 6 f and g. These findings suggest the opportunity to tune the load-bearing performance of the porous alloys by refining the ligaments' microstructure down to the nanoscale regime as well as employing the solid solution strengthening.

To study the effect of chemical composition on the mechanical behavior of the porous TiZr alloys, the set of samples shown in Fig. 7 b was fabricated. It has to be emphasized that it was not possible to synthesize porous TiZr alloys with identical solid fraction, starting with the same Cu content and following the same processing route. The chemical composition of precursors affects the solid fraction of dealloyed alloys, e.g. through different shrinkage behavior (Table 1). Summarizing the findings from that part of the investigations, the highest σ_y value was achieved for an equiatomic TiZr composition. Comparing σ_y values

between TiZr@63vol% (259 MPa) and Ti₇₅Zr₂₅@70vol% (136 MPa) allows concluding that the solid solution strengthening significantly dominates over the solid fraction effect in this case.

Application perspectives

The liquid metal dealloying-based porous alloys and their interpenetrating-phase composites represent a relatively new class of engineering materials [22]. These materials are distinguished due to their unique combination of mechanical properties demonstrating a strong deviation from the scaling relation between strength and stiffness usual for classical engineering materials. In particular, the $\sigma_{0.2}$ and Y values of the porous Ti_xZr_{100-x} materials of this study covers a substantial area of the “empty space” on the Ashby type diagram [52] in the area of intermediate (rather high) strength and low stiffness (Fig. 10). Exhibiting strength characteristics of even bulk alloys, the porous Ti_xZr_{100-x} alloys are possessing Young’s moduli comparable to that of cortical bone even without an infiltration of the pore space by another material. This suggests opportunities for the materials to be used as advanced materials for load bearing implant application. Furthermore, preliminary biological tests highlighted the materials cytocompatibility and a certain advantage of porous TiZr alloys over conventional Ti-6Al-4V alloy. Thus, effort should be pursued on further biological characterizations of the porous Ti_xZr_{100-x} alloys fabricated by liquid metal dealloying.

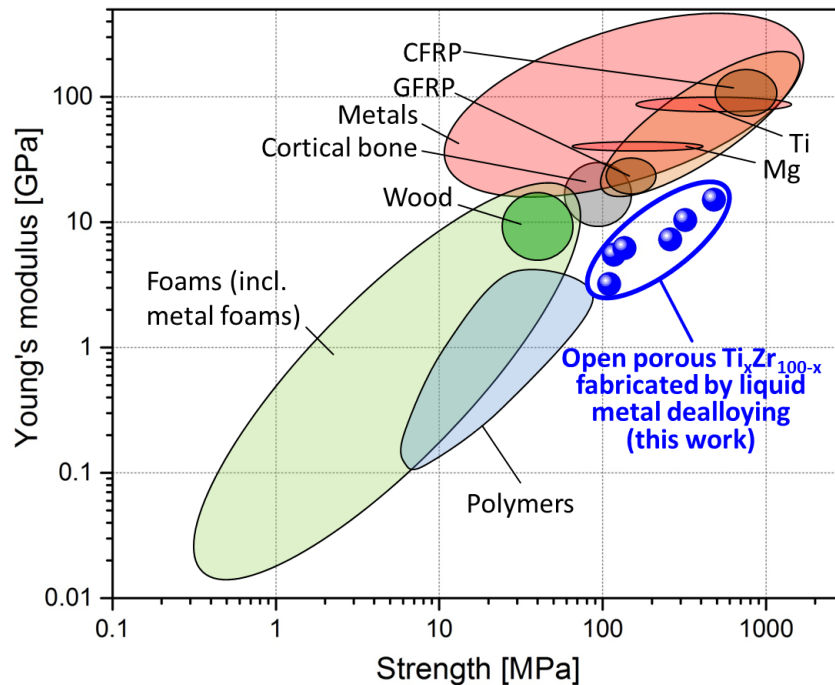


Figure 10 Ashby diagram of Young’s modulus plotted against yield strength demonstrating the unique combination of properties of the porous TiZr alloys favorable for load-bearing implant applications.

Conclusions

In summary, we presented the liquid metal dealloying method for fabrication of open porous metallic biomaterials with flexibly tunable properties. These dealloying-based materials enable development of a novel biomaterial platform. For demonstration here, several open porous $\text{Ti}_x\text{Zr}_{100-x}$ alloys were synthesized by means of the liquid metal dealloying of $(\text{Ti}_x\text{Zr}_{100-x})_y\text{Cu}_{100-y}$ precursors using Mg as the corrosive medium. The effects of dealloying conditions as well as chemical composition of the $(\text{Ti}_x\text{Zr}_{100-x})_y\text{Cu}_{100-y}$ precursors on the dealloyed microstructure of the porous $\text{Ti}_x\text{Zr}_{100-x}$ were studied. In particular, increasing dealloying time (from 5 to 20 min) and temperature (from 1073 to 1173 K) for the $(\text{TiZr})_{30}\text{Cu}_{70}$ precursor, generally, leads to coarsening of the microstructure, e.g. increasing thickness of ligaments. The decreasing Cu content in the $(\text{TiZr})_y\text{Cu}_{100-y}$ precursors from 70 to 40 at.% results in a higher solid fraction of the final porous TiZr reaching up to 79 vol%. The varying chemical composition, namely ratio of Ti to Zr in the $(\text{Ti}_x\text{Zr}_{100-x})_{40}\text{Cu}_{60}$ precursors, leads to a different ligament size and a different solid fraction of the porous $\text{Ti}_x\text{Zr}_{100-x}$ alloys. Thus, the microstructure of the dealloying-based porous $\text{Ti}_x\text{Zr}_{100-x}$ can be tuned by optimizing chemical composition of precursors as well as by control of the dealloying conditions.

The porous $\text{Ti}_x\text{Zr}_{100-x}$ alloys are distinguishing themselves from other porous metals due to their high yield strength reaching up to 480 MPa, an excellent compressive deformability and a low Young's modulus of about 15.1 GPa even in the case of high metal fractions of about 79 vol%. The yield strength strongly depends on solid fraction and chemical composition of the porous $\text{Ti}_x\text{Zr}_{100-x}$ alloys. For example, the yield strength can be tuned from 110 MPa to 480 MPa by varying the solid fraction from 49 vol% to 79 vol%. In terms of chemical composition, the dealloying-based porous $\text{Ti}_x\text{Zr}_{100-x}$ possessing an equiatomic composition is the strongest among the current set of samples. The overall high strength of the porous TiZr alloys is due to solid solution strengthening effect as well as the ultrafine-grained microstructure of their ligaments. The unique combination of mechanical properties of the dealloying-based porous alloys together with promising preliminary biological tests results indicates opportunities for load-bearing implant applications.

Acknowledgement

The authors would like to thank Sviatlana Lamaka and Gert Wiese for technical assistance and fruitful discussions. The funding by the Helmholtz Impuls- und Vernetzungsfonds via the Helmholtz - Chinese Academy of Sciences Joint Research Group "Nanoporous transition metals for strength and function – towards a cost-efficient materials base" grant no. HCJRG-315 and by the International Collaboration Center, Institute for Materials Research (ICC-IMR), Tohoku University, Japan are gratefully acknowledged.

Literature:

- [1] M. Geetha, A.K. Singh, R. Asokamani, A.K. Gogia, Ti based biomaterials, the ultimate choice for orthopaedic implants – A review, *Prog. Mater. Sci.* 54 (2009) 397–425. doi:10.1016/j.pmatsci.2008.06.004.
- [2] M. Niinomi, M. Nakai, J. Hieda, Development of new metallic alloys for biomedical applications., *Acta Biomater.* 8 (2012) 3888–903. doi:10.1016/j.actbio.2012.06.037.
- [3] M. Niinomi, T. Hattori, K. Morikawa, T. Kasuga, A. Suzuki, H. Fukui, S. Niwa, Development of Low Rigidity Beta-type Titanium Alloy for Biomedical Applications., *Mater. Trans.* 43 (2002) 2970–2977. doi:10.2320/matertrans.43.2970.
- [4] H. Attar, S. Ehtemam-haghighi, D. Kent, I. V Okulov, H. Wendrock, M. B, A.S. Volegov, M. Calin, J. Eckert, M.S. Dargusch, Nanoindentation and wear properties of Ti and Ti-TiB composite materials produced by selective laser melting, *Mater. Sci. Eng. A.* 688 (2017) 20–26. doi:10.1016/j.msea.2017.01.096.
- [5] H. Attar, K.G. Prashanth, L.-C. Zhang, M. Calin, I. V. Okulov, S. Scudino, C. Yang, J. Eckert, Effect of Powder Particle Shape on the Properties of In Situ Ti–TiB Composite Materials Produced by Selective Laser Melting, *J. Mater. Sci. Technol.* 31 (2015) 1001–1005. doi:10.1016/j.jmst.2015.08.007.
- [6] I.V. Okulov, M.F. Sarmanova, A.S. Volegov, A. Okulov, U. Kühn, W. Skrotzki, J. Eckert, Effect of boron on microstructure and mechanical properties of multicomponent titanium alloys, *Mater. Lett.* 158 (2015) 111–114. doi:10.1016/j.matlet.2015.06.017.
- [7] W. Skrotzki, A. Eschke, J. Romberg, J. Scharnweber, T. Marr, R. Petters, I. Okulov, C.-G. Oertel, J. Freudenberger, U. Kühn, L. Schultz, J. Eckert, Processing of High Strength Light-Weight Metallic Composites, *Adv. Eng. Mater.* 16 (2014). doi:10.1002/adem.201400190.
- [8] T. Marr, J. Freudenberger, A. Kauffmann, J. Romberg, I. Okulov, R. Petters, J. Scharnweber, A. Eschke, C.-G. Oertel, U. Kühn, J. Eckert, W. Skrotzki, L. Schultz, Processing of Intermetallic Titanium Aluminide Wires, *Metals (Basel)*. 3 (2013) 188–201. doi:10.3390/met3020188.
- [9] T. Marr, J. Freudenberger, D. Seifert, H. Klauß, J. Romberg, I. Okulov, J. Scharnweber, A. Eschke, C.-G. Oertel, W. Skrotzki, U. Kühn, J. Eckert, L. Schultz, Ti-Al Composite Wires with High Specific Strength, *Metals (Basel)*. 1 (2011) 79–97. doi:10.3390/met1010079.
- [10] M. Nakai, M. Niinomi, T. Akahori, H. Tsutsumi, S. Itsuno, N. Haraguchi, Y. Itoh, T. Ogasawara, Development of biomedical porous titanium filled with medical polymer by in-situ polymerization of monomer solution infiltrated into pores, *J. Mech. Behav. Biomed. Mater.* 3 (2010) 41–50. doi:10.1016/j.jmbbm.2009.03.003.
- [11] I.V. Okulov, U. Kühn, T. Marr, J. Freudenberger, I.V. Soldatov, L. Schultz, C.-G. Oertel, W. Skrotzki, J. Eckert, Microstructure and mechanical properties of new composite structured Ti–V–Al–Cu–Ni alloys for spring applications, *Mater. Sci. Eng. A.* 603 (2014) 76–83. doi:10.1016/j.msea.2014.02.070.
- [12] I.V. Okulov, H. Wendrock, A.S. Volegov, H. Attar, U. Kühn, W. Skrotzki, J. Eckert, High strength beta titanium alloys: New design approach, *Mater. Sci. Eng. A.* 628 (2015) 297–302.

doi:10.1016/j.msea.2015.01.073.

- [13] I.V. Okulov, S. Pauly, U. Kühn, P. Gargarella, T. Marr, J. Freudenberger, L. Schultz, J. Scharnweber, C.-G. Oertel, W. Skrotzki, J. Eckert, Effect of microstructure on the mechanical properties of as-cast Ti–Nb–Al–Cu–Ni alloys for biomedical application, *Mater. Sci. Eng. C*. 33 (2013) 4795–4801. doi:10.1016/j.msec.2013.07.042.
- [14] I. V. Okulov, U. Kühn, T. Marr, J. Freudenberger, L. Schultz, C.-G. Oertel, W. Skrotzki, J. Eckert, Deformation and fracture behavior of composite structured Ti-Nb-Al-Co(-Ni) alloys, *Appl. Phys. Lett.* 104 (2014) 71905. doi:10.1063/1.4865930.
- [15] I. V Okulov, A.S. Volegov, H. Attar, M. Bönisch, M. Calin, J. Eckert, Composition optimization of low modulus and high-strength TiNb-based alloys for biomedical applications, *J. Mech. Behav. Biomed. Mater.* 65 (2017) 866–871. doi:10.1016/j.jmbbm.2016.10.013.
- [16] I.V. Okulov, M. Bönisch, A.S. Volegov, H. Shahabi Shakur, H. Wendrock, T. Gemming, J. Eckert, Micro-to-nano-scale deformation mechanism of a Ti-based dendritic-ultrafine eutectic alloy exhibiting large tensile ductility, *Mater. Sci. Eng. A*. (2016). doi:10.1016/j.msea.2016.11.082.
- [17] I.V. Okulov, M. Bönisch, U. Kühn, W. Skrotzki, J. Eckert, Significant tensile ductility and toughness in an ultrafine-structured Ti68.8Nb13.6Co6Cu5.1Al6.5 bi-modal alloy, *Mater. Sci. Eng. A*. 615 (2014) 457–463. doi:10.1016/j.msea.2014.07.108.
- [18] I.V. Okulov, U. Kühn, J. Romberg, I.V. Soldatov, J. Freudenberger, L. Schultz, A. Eschke, C.-G. Oertel, W. Skrotzki, J. Eckert, Mechanical behavior and tensile/compressive strength asymmetry of ultrafine structured Ti–Nb–Ni–Co–Al alloys with bi-modal grain size distribution, *Mater. Des.* 62 (2014) 14–20. doi:10.1016/j.matdes.2014.05.007.
- [19] I. V. Okulov, I. V. Soldatov, M.F. Sarmanova, I. Kaban, T. Gemming, K. Edström, J. Eckert, Flash Joule heating for ductilization of metallic glasses, *Nat. Commun.* 6 (2015) 7932. doi:10.1038/ncomms8932.
- [20] B.J.C. Luthringer, F. Ali, H. Akaichi, F. Feyerabend, T. Ebel, R. Willumeit, Production , characterisation , and cytocompatibility of porous titanium-based particulate scaffolds, (2013) 2337–2358. doi:10.1007/s10856-013-4989-z.
- [21] K.G. Prashanth, K. Zhuravleva, I. Okulov, M. Calin, J. Eckert, A. Gebert, Mechanical and Corrosion Behavior of New Generation Ti-45Nb Porous Alloys Implant Devices, *Technologies*. 4 (2016) 33. doi:10.3390/technologies4040033.
- [22] I. V Okulov, J. Weissmüller, J. Markmann, Dealloying-based interpenetrating-phase nanocomposites matching the elastic behavior of human bone, *Sci. Rep.* 7 (2017) 20. doi:10.1038/s41598-017-00048-4.
- [23] T. Wada, K. Yubuta, A. Inoue, H. Kato, Dealloying by metallic melt, *Mater. Lett.* 65 (2011) 1076–1078. doi:10.1016/j.matlet.2011.01.054.
- [24] M. Tsuda, T. Wada, H. Kato, Kinetics of formation and coarsening of nanoporous α -titanium dealloyed with Mg melt, *J. Appl. Phys.* 114 (2013). doi:10.1063/1.4821066.
- [25] T. Wada, H. Kato, Three-dimensional open-cell macroporous iron, chromium and ferritic stainless

- steel, *Scr. Mater.* 68 (2013) 723–726. doi:10.1016/j.scriptamat.2013.01.011.
- [26] J.W. Kim, M. Tsuda, T. Wada, K. Yubuta, S.G. Kim, H. Kato, Optimizing niobium dealloying with metallic melt to fabricate porous structure for electrolytic capacitors, *Acta Mater.* 84 (2015) 497–505. doi:10.1016/j.actamat.2014.11.002.
- [27] A.V. Okulov, A.S. Volegov, J. Weissmüller, J. Markmann, I.V. Okulov, Dealloying-based metal-polymer composites for biomedical applications, *Scr. Mater.* 146 (2018) 290–294. doi:10.1016/j.scriptamat.2017.12.022.
- [28] S.G. Yu, K. Yubuta, T. Wada, H. Kato, Three-dimensional bicontinuous porous graphite generated in low temperature metallic liquid, *Carbon N. Y.* 96 (2016) 403–410. doi:10.1016/j.carbon.2015.09.093.
- [29] I. McCue, S. Ryan, K. Hemker, X. Xu, N. Li, M. Chen, J. Erlebacher, Size Effects in the Mechanical Properties of Bulk Bicontinuous Ta/Cu Nanocomposites Made by Liquid Metal Dealloying, *Adv. Eng. Mater.* 18 (2016) 46–50. doi:10.1002/adem.201500219.
- [30] I. McCue, B. Gaskey, P.A. Geslin, A. Karma, J. Erlebacher, Kinetics and morphological evolution of liquid metal dealloying, *Acta Mater.* 115 (2016) 10–23. doi:10.1016/j.actamat.2016.05.032.
- [31] T. Wada, A.D. Setyawan, K. Yubuta, H. Kato, Nano- to submicro-porous β -Ti alloy prepared from dealloying in a metallic melt, *Scr. Mater.* 65 (2011) 532–535. doi:10.1016/j.scriptamat.2011.06.019.
- [32] K. Sasaki, S. Osamu, N. Takahashi, Interface oral health science 2014: Innovative research on biosis-abiosis intelligent interface, *Interface Oral Heal. Sci. 2014 Innov. Res. Biosis-Abiosis Intell. Interface.* (2015) 1–351. doi:10.1007/978-4-431-55192-8.
- [33] A.B. Novaes, S.L.S. de Souza, R.R.M. de Barros, K.K.Y. Pereira, G. Iezzi, A. Piattelli, Influence of implant surfaces on osseointegration, *Braz. Dent. J.* 21 (2010) 471–481. doi:http://dx.doi.org/10.1590/S0103-64402010000600001.
- [34] H.M. Grandin, S. Berner, M. Dard, A Review of Titanium Zirconium (TiZr) Alloys for Use in Endosseous Dental Implants, (2012) 1348–1360. doi:10.3390/ma5081348.
- [35] A. Takeuchi, A. Inoue, Metallic Glasses By Atomic Size Difference, Heat of Mixing and Period of Constituent Elements and Its Application To Characterization of the Main Alloying Element, *Mater. Trans.* 46 (2005) 2817–2829. doi:10.2320/matertrans.46.2817.
- [36] M. Calin, A. Gebert, A.C. Ghinea, P.F. Gostin, S. Abdi, C. Mickel, J. Eckert, Designing biocompatible Ti-based metallic glasses for implant applications, *Mater. Sci. Eng. C.* 33 (2013) 875–883. doi:10.1016/j.msec.2012.11.015.
- [37] J.B. Park, J.D. Bronyino, *Biomaterials: principles and applications*, 2nd ed., CRC Press, Boca Raton, 2000.
- [38] H. Matsuno, A. Yokoyama, F. Watari, M. Uo, T. Kawasaki, Biocompatibility and osteogenesis of refractory metal implants, titanium, hafnium, niobium, tantalum and rhenium, *Biomaterials.* 22 (2001) 1253–1262. doi:https://doi.org/10.1016/S0142-9612(00)00275-1.

- [39] E. Eisenbarth, D. Velten, M. Müller, R. Thull, J. Breme, Biocompatibility of β -stabilizing elements of titanium alloys, *Biomaterials*. 25 (2004) 5705–5713. doi:10.1016/j.biomaterials.2004.01.021.
- [40] D. Kuroda, M. Niinomi, M. Morinaga, Y. Kato, T. Yashiro, Design and mechanical properties of new beta type titanium alloys for implant materials, *Mater. Sci. Eng. A243*. (1998) 244–249. doi:10.1016/S0921-5093(97)00808-3.
- [41] P. Geslin, I. Mccue, J. Erlebacher, A. Karma, Topology-generating interfacial pattern formation during liquid metal dealloying, *Nat. Commun.* 6 (2015) 1–19. doi:10.1038/ncomms9887.
- [42] H. Umbilical, C. Perivascular, H. Cells, R. Sarugaser, D. Lickorish, D. Baksh, M.M. Hosseini, J.E. Davies, Human umbilical cord perivascular (HUCPV) cells: a source of mesenchymal progenitors., *Stem Cells*. 23 (2005) 220–229. doi:10.1634/stemcells.2004-0166.
- [43] S. Sun, X. Chen, N. Badwe, K. Sieradzki, Potential-dependent dynamic fracture of nanoporous gold, *Nat. Mater.* 14 (2015) 894–899. doi:10.1038/NMAT4335.
- [44] E. Kobayashi, S. Matsumoto, H. Doi, T. Yoneyama, H. Hamanaka, Mechanical properties of the binary titanium-zirconium alloys and their potential for biomedical materials, *J. Biomed. Mater. Res.* 29 (1995) 943–950. doi:10.1002/jbm.820290805.
- [45] C. Leyens, M. Peters, *Titanium and Titanium Alloys*, WILEY-VCH Verlag GmbH & Co. KGaA, Weinheim, 2003.
- [46] G. Lütjering, J. C. Williams, *Titanium*, Springer, Berlin, 2007.
- [47] K. Wang, J. Weissmüller, Composites of nanoporous gold and polymer, *Adv. Mater.* 25 (2013) 1280–1284. doi:10.1002/adma.201203740.
- [48] R.E. Smallman, R.J. Bishop, Chapter 13 - Biomaterials, in: R.E. Smallman, R.J. Bishop (Eds.), *Mod. Phys. Metall. Mater. Eng.* (Sixth Ed., Sixth edit, Butterworth-Heinemann, Oxford, 1999: pp. 394–405. doi:http://dx.doi.org/10.1016/B978-075064564-5/50013-6.
- [49] N. Mameka, K. Wang, J. Markmann, E.T. Lilleodden, J. Weissmüller, Nanoporous Gold—Testing Macro-scale Samples to Probe Small-scale Mechanical Behavior, *Mater. Res. Lett.* 3831 (2015) 1–10. doi:10.1080/21663831.2015.1094679.
- [50] L. Liu, X. Ye, H. Jin, *Acta Materialia* Interpreting anomalous low-strength and low-stiffness of nanoporous gold : Quantification of network connectivity, *Acta Mater.* 118 (2016) 77–87. doi:10.1016/j.actamat.2016.07.033.
- [51] M. Nakai, M. Niinomi, D. Ishii, Mechanical and biodegradable properties of porous titanium filled with poly-L-lactic acid by modified in situ polymerization technique, *J. Mech. Behav. Biomed. Mater.* 4 (2011) 1206–1218. doi:10.1016/j.jmbbm.2011.04.003.
- [52] M.F. Ashby, *Materials Selection in Mechanical Design*, 3rd ed., Butterworth-Heinemann, 2005.